Materials & Design 83 (2015) 387–399

Contents lists available at ScienceDirect

Materials & Design

journal homepage: www.elsevier.com/locate/matdes

# The mechanical properties of ionoplast interlayer material at high strain rates

Xihong Zhang [a,*], Yanchao Shi [b], Hong Hao [a], Jian Cui [b]

[a] Centre for Infrastructural Monitoring and Protection, School of Civil and Mechanical Engineering, Curtin University, Kent St., Bentley, WA 6102, Australia
[b] Tianjin University and Curtin University Joint Research Center of Structural Monitoring and Protection, Tianjin University, China

ARTICLE INFO

*Article history:*
Received 20 November 2014
Revised 13 May 2015
Accepted 8 June 2015
Available online 19 June 2015

*Keywords:*
Ionoplast interlayer
SGP
Dynamic material property
Strain rate effect

ABSTRACT

Ionoplast material has been recently introduced and extensively used as interlayer material for laminated glass to improve its post-glass breakage behavior. Due to its sound mechanical performance, the applications of laminated glass with ionoplast interlayer have been widely extended to the protection of glass structures against extreme loads such as shock and impact. The properties of this material at high strain rates are therefore needed for properly analysis and design of such structures. In this study, the mechanical properties of ionoplast material are studied experimentally through direct tensile tests over a wide strain rate range. The low-speed tests are performed using a conventional hydraulic machine at strain rates from 0.0056 $s^{-1}$ to 0.556 $s^{-1}$. The high strain-rate tests are carried out with a high-speed servo-hydraulic testing machine at strain rates from approximately 10 $s^{-1}$ to 2000 $s^{-1}$. It is found that the ionoplast material virtually exhibits elasto-plastic material properties in the strain rate range tested in this study. The testing results show that the material behavior is very strain-rate dependent. The yield strength increases with strain rate, but the material becomes more brittle with the increase in strain rate, with the ultimate strains over 400% under quasi-static loading, and decreasing to less than 200% at strain rate around 2000 $s^{-1}$. The testing results indicate that simply applying the static material properties in predicting the structure responses of laminated glass with ionoplast interlayer subjected to blast and impact loads will substantially overestimate the ductility of the material and lead to inaccurate predictions of structure response. The testing results obtained in the current study together with available testing data in the literature are summarized and used to formulate the dynamic stress–strain curves of ionoplast material at various strain rates, which can be used in analysis and design of structures with ionoplast material subjected to blast and impact loads.



## 1. Introduction

Because of the increased threats from windborne debris impacts on glass windows owing to the increased wind speed with climate change, and the increased threats of bombing attacks owing to the increased terrorism activities, protection of glass windows against impact and blast loads is critical for people protection since glass windows are the relatively weaker sections in a structure, and glass fragments have been identified as the source for most casualties in such events [1,2]. Laminated glass windows have been proved effective for mitigating glass fragment threats as compared to the monolithic glass windows [2–7]. The most commonly used interlayer material for laminated glass, polyvinyl butyral (PVB), is soft, very ductile and exhibits viscoelastic material properties. After glass breakage, PVB interlayer will stick the shattered glass fragments together therefore prevent them from flying into the room. The interlayer material with large ductility will continue to deform and dissipate the imposed energy. However, due to the limited stiffness and strength of PVB, laminated glass with PVB interlayer offers relatively poor residual load-carrying capacity after glass breakage [8]. Rupture of PVB under large blast and impact loads results in the complete collapse of the window structure and lead to the failed interlayer and shattered glass fragments flying together into the room. Therefore, materials stronger and more ductile than PVB that can be used as interlayer material in laminated glass are constantly sought.

SentryGlas®Plus (SGP) by DuPont® is a well-known and commonly used ionoplast material for the replacement of PVB interlayer. As an ionoplast material, SGP primarily comprises of ethylene/methacrylic acid copolymers. It also contains small

* Corresponding author.
*E-mail address:* xihong.zhang@curtin.edu.au (X. Zhang).

http://dx.doi.org/10.1016/j.matdes.2015.06.076
0264-1275/

amounts of metal salts which improves its bonding performance to glass ply. SGP behaves elasto-plastically under tensile loading. It is stated to offer up to five times the tearing strength and a hundred times the rigidity of conventional PVB material. As a result, SGP is more and more commonly used as the interlayer in protective designs of glass structures.

Understanding the mechanical properties of SGP material at different strain rates is of great importance for reliable analysis and design of glass structures because the laminated glass structure might be subjected to loads of different rates, ranging from quasi-static to high-rate impact and blast loads. Belis et al. [8] conducted uniaxial tensile tests on 25 SGP specimens at five loading speeds in the quasi-static range. The testing results revealed an elasto-plastic behavior of SGP. It was found that the yield stress is amplified when the loading speed increases. Similar observation was reported by Bennison et al. [9]. Using a servo-hydraulic testing machine, Bennison and his co-workers tested SGP specimens in the strain rate range from 0.1 $s^{-1}$ up to 125 $s^{-1}$. The yield stress was found to increase from about 31 MPa to 36 MPa. It was also revealed that the ultimate strain of SGP decreased with the strain rate [9]. The dynamic material property of SGP at other strain rates especially at strain rates above 100 $s^{-1}$ has not been widely reported in the literature yet.

In this study, the mechanical properties of ionoplast material SGP under the tensile loading at various strain rates are investigated experimentally. SGP specimens are firstly pulled at low speeds to study its behavior under quasi-static loading conditions. High-speed servo-hydraulic machine is then employed to carry out high-speed tensile tests on SGP specimens. The responses of SGP material at strain rates from approximately 10 $s^{-1}$ to 2000 $s^{-1}$ are investigated. The deformation-to-fracture behavior of SGP material is monitored by a high-speed camera. The stress–strain curves of SGP material are presented and analyzed. The results obtained in this study can be used to model SGP material behavior under different strain rates.

## 2. Theory and methodology

### 2.1. Testing systems

Experimental techniques commonly used to determine the material tensile properties at different strain rates include conventional screw driven load frame, servo-hydraulic machine, pendulum or drop weight impact machine, high-speed servo-hydraulic machine, and Split-Hopkinson Pressure Bar system. The conventional testing systems including the screw driven load frame and conventional servo-hydraulic machine can normally test material tensile strength at a strain rate up to 1 $s^{-1}$. Split-Hopkinson Pressure Bar (SHPB) is commonly used to determine the material strength at high strain rates ($\dot{\varepsilon} \geqslant 100\ s^{-1}$). To test the material tensile properties, the tensile SHPB usually requires the testing specimen to be firmly glued on both ends respectively to the incident and transmitter bars to ensure the tensile stress wave can travel through the specimen before it fractures. It is therefore not suitable for polymer materials such as SGP, as the glue could significantly alter the material properties. The pendulum or drop weight impact system and the high-speed servo-hydraulic machine have been widely used to determine material strength at strain rate above 1 $s^{-1}$. Dumbbell shaped specimens similar to those used for quasi-static tests are most commonly adopted for the dynamic tensile tests. Due to the inherent difficulties, the strain rates that can be achieved by a drop weight impact machine is usually restricted by the drop height and therefore limited to 1–100 $s^{-1}$. Moreover, during a test the velocity of the actuator is also coupled with the response of the specimen. In other words, it is difficult for the drop weight impactor to maintain a constant testing velocity. In this study, servo-hydraulic and high-speed servo-hydraulic machines are used to perform the low-speed and high-speed tensile tests. The testing setups and machine information are described in details in section three and four.


**Fig. 1.** INSTRON hydraulic machine for low-speed test.

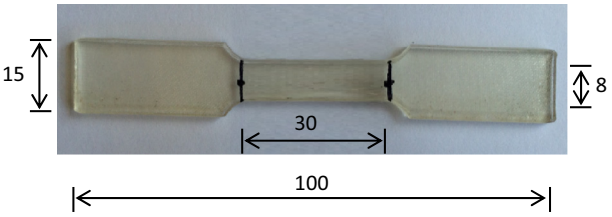


**Fig. 2.** Illustration of specimen geometry for low-speed test.

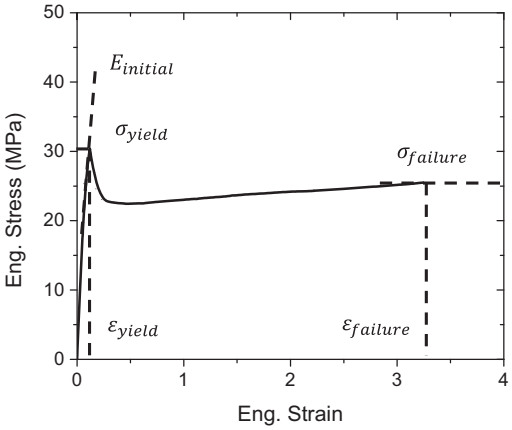


**Fig. 3.** Typical engineering stress–strain curve for SGP material.

### 2.2. Testing requirements for high-speed tests

To ensure the validity of testing data for a material test, it is critical to assure the specimen is under the state of stress equilibrium. For low-speed tests, the specimens are in quasi-static equilibrium,

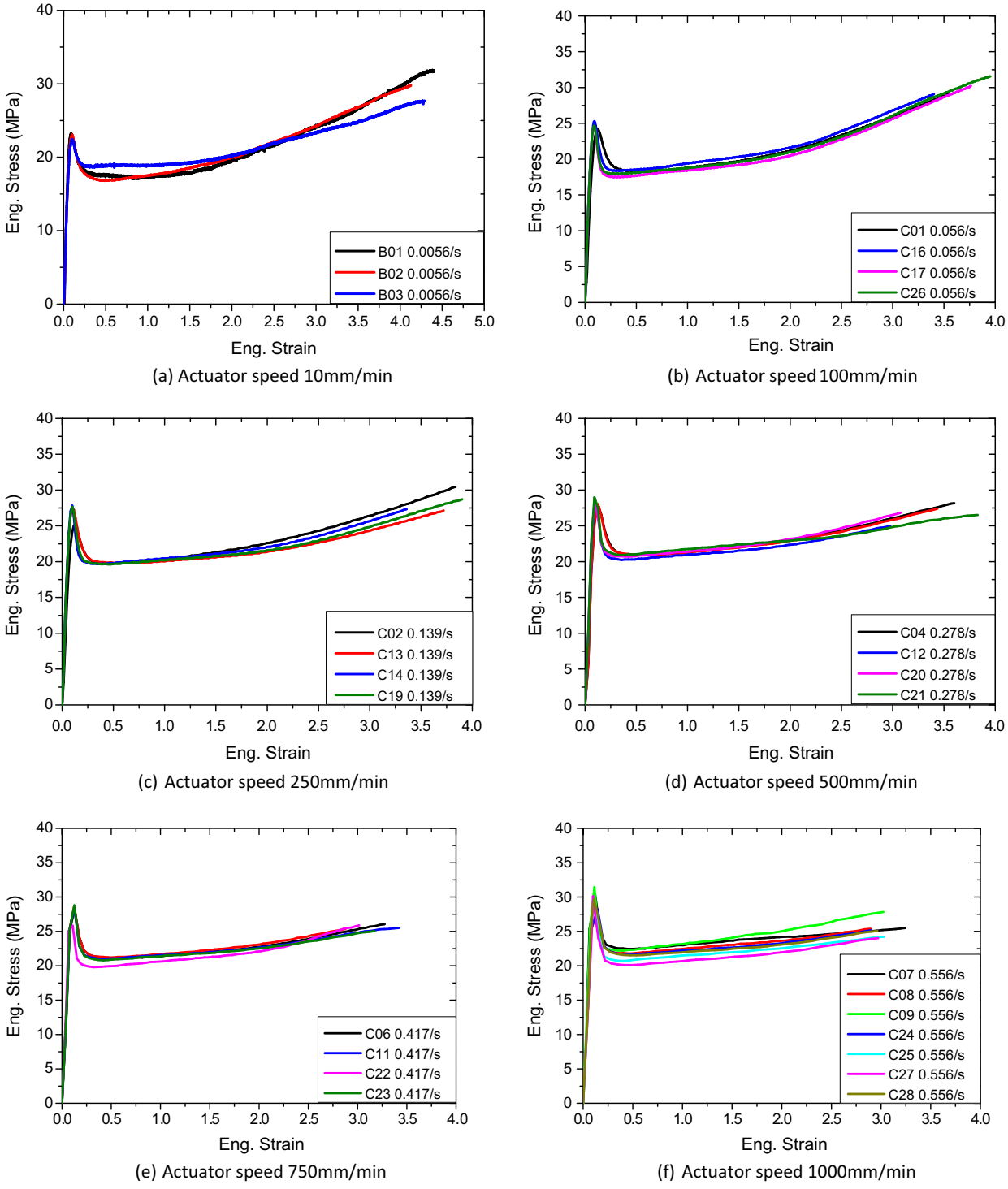


**Fig. 4.** Stress–strain curves from low-speed SGP tensile tests at different strain rates.

because there is more than sufficient time for elastic waves to travel back and forth many times in the specimen in the loading duration. For high-speed tests, to achieve the state of stress equilibrium is much more difficult since the loading time can be much shorter. In a dynamic test, a state of dynamic equilibrium is usually pursued, where a minimum number of elastic waves are required to propagate through the specimen. To estimate the time for one stress wave to travel a round trip in the specimen the following relation can be utilized

$$t = \frac{2L}{c} \tag{1}$$

where $L$ is the specimen length between the clamping grips; and $c$ is the elastic stress wave velocity in the specimen material. The one-dimensional longitudinal wave velocity in an isotropic material can be estimated by the relation

$$c = \sqrt{\frac{E}{\rho}} \tag{2}$$

**Table 1**
Summary of low speed tensile testing results.

| Specimen no. | Actuator speed (mm/min) | Strain rate ($s^{-1}$) | Eng. $\sigma_{yield}$ (MPa) | Eng. $\varepsilon_{yield}$ | $E_{initial}$ (MPa) | Eng. $\sigma_{failure}$ (MPa) | Eng. $\varepsilon_{failure}$ |
|---|---|---|---|---|---|---|---|
| B01 | 10 | 0.006 | 22.90 | 0.09 | 243.86 | 29.81 | 4.13 |
| B02 | 10 | 0.006 | 23.17 | 0.10 | 243.17 | 31.86 | 4.40 |
| B03 | 10 | 0.006 | 22.43 | 0.10 | 230.50 | 27.72 | 4.29 |
| C01 | 100 | 0.056 | 24.19 | 0.12 | 194.03 | 29.07 | 3.55 |
| C16 | 100 | 0.056 | 25.29 | 0.09 | 275.24 | 29.08 | 3.40 |
| C17 | 100 | 0.056 | 24.51 | 0.09 | 287.14 | 30.22 | 3.76 |
| C26 | 100 | 0.056 | 24.65 | 0.09 | 288.70 | 31.56 | 3.95 |
| C02 | 250 | 0.139 | 25.01 | 0.12 | 203.17 | 30.45 | 3.84 |
| C13 | 250 | 0.139 | 27.25 | 0.10 | 296.85 | 27.13 | 3.72 |
| C14 | 250 | 0.139 | 27.81 | 0.10 | 281.88 | 27.81 | 3.36 |
| C19 | 250 | 0.139 | 27.66 | 0.10 | 280.30 | 28.72 | 3.90 |
| C04 | 500 | 0.278 | 27.97 | 0.13 | 222.26 | 28.17 | 3.60 |
| C05 | 500 | 0.278 | 28.01 | 0.13 | 223.12 | 28.01 | 3.44 |
| C12 | 500 | 0.278 | 28.23 | 0.09 | 302.32 | 28.23 | 2.98 |
| C20 | 500 | 0.278 | 28.80 | 0.10 | 270.73 | 26.84 | 3.08 |
| C21 | 500 | 0.278 | 28.97 | 0.09 | 315.84 | 28.97 | 3.83 |
| C06 | 750 | 0.417 | 28.24 | 0.13 | 221.46 | 28.24 | 3.27 |
| C10 | 750 | 0.417 | 28.68 | 0.12 | 230.20 | 28.68 | 2.88 |
| C11 | 750 | 0.417 | 28.50 | 0.13 | 226.96 | 28.50 | 3.42 |
| C22 | 750 | 0.417 | 25.82 | 0.13 | 200.82 | 25.90 | 3.02 |
| C23 | 750 | 0.417 | 28.79 | 0.13 | 229.23 | 28.79 | 3.17 |
| C07 | 1000 | 0.556 | 30.38 | 0.14 | 213.97 | 25.51 | 3.25 |
| C08 | 1000 | 0.556 | 27.87 | 0.14 | 193.62 | 27.87 | 2.90 |
| C09 | 1000 | 0.556 | 31.45 | 0.11 | 278.11 | 27.83 | 3.02 |
| C24 | 1000 | 0.556 | 28.20 | 0.15 | 194.15 | 28.20 | 2.90 |
| C25 | 1000 | 0.556 | 29.27 | 0.10 | 314.61 | 25.21 | 3.03 |
| C27 | 1000 | 0.556 | 30.13 | 0.10 | 288.35 | 25.13 | 2.97 |
| C28 | 1000 | 0.556 | 29.66 | 0.11 | 189.57 | 27.53 | 2.96 |

where $\rho$ is the density of the material and $E$ is the Young's modulus.

To reach dynamic stress equilibrium, a SHPB test normally requires at least three reverberations of the loading wave in the specimen [10,11]. Based on the experience gained through dynamic tensile tests using a high-speed servo-hydraulic machine on four plastic materials (HDPE, PC-ABS, TPO and PP/glass) Xiao [12] found the criterion for a valid SHPB test is also applicable to dynamic direct tensile test. The draft standard of the Society of Automotive Engineers on high strain-rate tensile test of automotive plastics requires at least 10 elastic reflected waves propagating through the specimen from the time of loading to the time of yield [13]. There is no quantitative criterion in the open literature yet defining the exact number of reflected stress wave in the specimen to achieve dynamic equilibrium for a uniaxial tensile test.

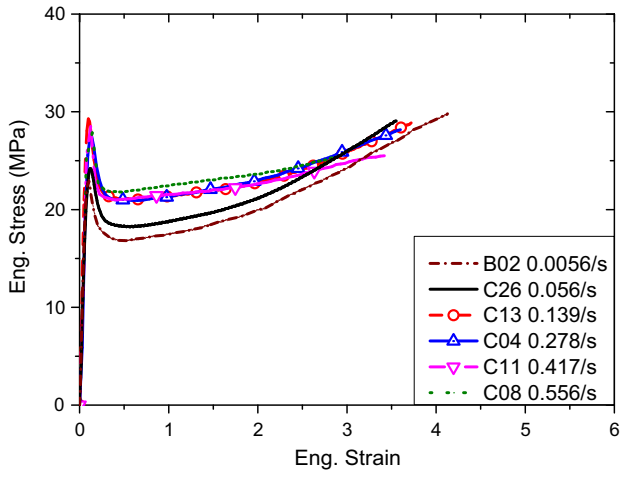


**Fig. 5.** Illustration of strain rate effect at low-speed tensile tests.

### 2.3. True stress for large deformation

In universal tensile test, due to the reduction in cross-sectional area, especially when the deformation level of the specimen is large, engineering stress is no longer an accurate measurement to describe the response of material. In such a circumstance, the true stress, which takes the changes of cross-sectional area into consideration, should be utilized. The true stress can be related to the engineering stress with the following expression

$$\sigma_t = \sigma_{eng}(1 + \varepsilon_{eng}) \tag{3}$$

where $\sigma_t$ is the true stress, $\sigma_{eng}$ and $\varepsilon_{eng}$ are the engineering stress and engineering strain.

Eq. (3) is derived by assuming that the strain is uniform and the deformation of material occurs with a constant volume. The assumption is valid for materials with a Poisson's ratio approximately equals to 0.5. According to DuPont®, SGP has a Poisson's ratio in the range of 0.45–0.5 under room temperature of 20–30 °C. The above equation to derive the true stress from engineering stress can therefore be used.

## 3. Low-speed tests

### 3.1. Test setup

The low-speed test was carried out in the mechanical laboratory at the University of Western Australia on an INSTRON hydraulic machine UTS-5982 (as shown in Fig. 1). The actuator of the machine is capable of traveling up to a maximum stroke of 1430 mm at a constant speed ranging from 0.00005 mm/min to 1016 mm/min. An inbuilt load cell and extensometer were used to measure the force and elongation that the specimens experienced. The room temperature during the test was about 25 ± 5 °C.

Fig. 2 illustrates the geometry of the SGP specimen for the low-speed test. The specimen has a dumbbell shape to assure homogenous deformation under tensile loading. The straight gauge has a length of 30 mm and a width of 8 mm. The specimens were machined from 2.28 mm SGP sheet. Due to the stiffness of the interlayer material, laser cutter was used to shape the specimens

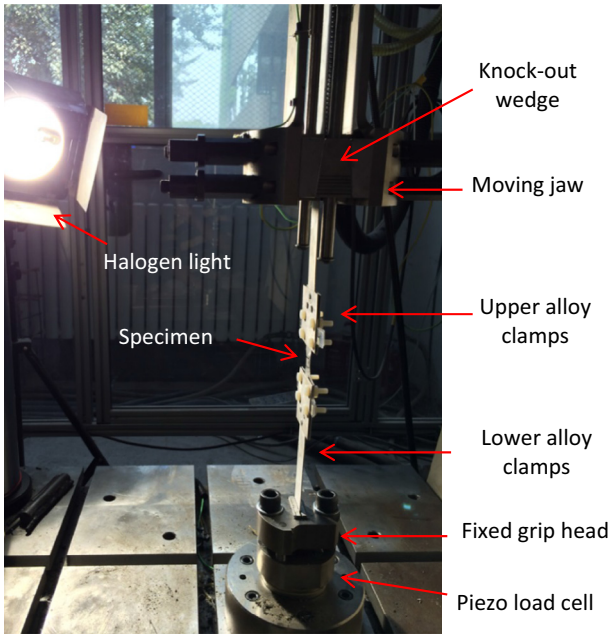


**Fig. 6.** High speed tensile test setup.

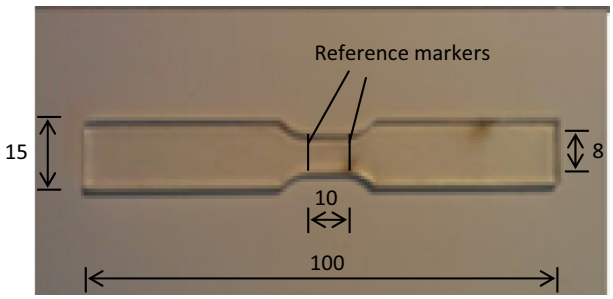


**Fig. 7.** Illustration of specimen geometry in the high-speed tensile test.

to the designed dimension. 27 specimens were tested at six crosshead velocities, i.e. 10, 100, 250, 500, 750, and 1000 mm/min, which correspond to nominal strain rates of 0.0056 $s^{-1}$, 0.056 $s^{-1}$, 0.139 $s^{-1}$, 0.278 $s^{-1}$, 0.417 $s^{-1}$, and 0.556 $s^{-1}$ on specimens (nominal strain rate derived with actuator speed divided by gauge length).

### 3.2. Low strain-rate testing results

Fig. 3 shows a typical stress–strain curve of a SGP specimen obtained in the low-speed test. As shown, the SGP specimen behaves essentially elasto-plastically under the uniaxial tensile loading. The material shows a steep increase in stress under the applied loading. After the stress reaches a peak value $\sigma_{yield}$ the load bearing capacity of the specimen drops. The strain corresponding to $\sigma_{yield}$ is defined as the yield strain, $\varepsilon_{yield}$, and the modulus for the initial part is named as the initial modulus, $E_{initial}$. As crosshead continues to move upward, the yielded SGP specimen elongates further overwhelmingly while the stress does not show a significant increase. The stress at failure, $\sigma_f$, and the corresponding strain, $\varepsilon_f$, are calculated at the instant that the specimen fractures.

Fig. 4 shows the engineering stress–strain curves for the SGP specimens tested at six different tensile speeds. It can be observed that at low strain rates (0.0056–0.556 $s^{-1}$) SGP material behaves virtually the same with a steep rise in stress at the beginning, followed with a substantial plastic deformation before failure. Table 1 summarizes the testing results of the SGP specimen at both yielding and failure. The behavior of SGP specimens show strain rate dependence. Fig. 5 shows the stress–strain curves of SGP specimens at different strain rates in the low-speed tensile tests. As shown, in general higher loading speeds correspond to higher yield stresses. When the strain rate is 0.0056 $s^{-1}$ the specimen yields at about 22.8 MPa. As strain rate increases to 0.278 $s^{-1}$, the yield stress becomes 28.8 MPa with a 26% increment. The strains at failure are in general above 300%. But as the strain rate increases, the failure strain tends to decrease. For instance, as shown in Fig. 5 the specimen fractures at strain 427% when the strain rate is 0.0056 $s^{-1}$. In comparison, the strain at fracture reduces to about 300% when strain rate is 0.556 $s^{-1}$.

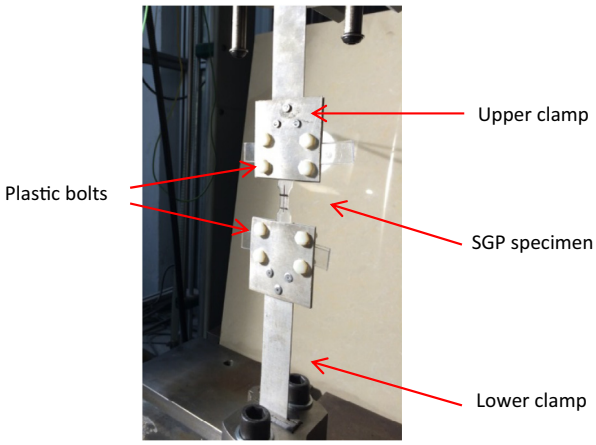


**Fig. 8.** Clamping devices for the high-speed tensile test.

## 4. High-speed dynamic tests

The high-speed tensile test was performed in the laboratory of Tianjin University and Curtin University Joint Research Centre. The room temperature during the test was about 30 ± 3 °C. A high-speed servo-hydraulic test machine was used to investigate the behavior of SGP materials with an actuator constant pulling speeds ranging from 0.1 m/s to 20 m/s. The dynamic material properties of SGP at strain rates ranging from approximately 10–2000 $s^{-1}$ were obtained.

### 4.1. Test setup

An INSTRON Very-High Strain-Rate Testing Machine (VHS 160-20) was used to perform the high-speed tensile test. The actuator of the machine can reach a constant testing velocity of up to 25 m/s under open loop control, and 1 mm/s to 1 m/s constant velocity under closed loop control. The machine has a moving jaw grip, which travels and accelerates upwards in the direction of tension (Fig. 6). Once it reaches the target testing velocity, a pre-set wedge is kicked out which releases the sprung grips to grab the specimen and pull it at the target velocity till the failure of specimen.

A piezo load cell was fixed below the bottom static grip head to measure the force transmitted to the testing specimen. A linear variable differential transducer (LVDT) mounted on the moving jaw was used to measure the actuator stroke in real time. A one-dimensional accelerometer was also mounted on the moving jaw to track the acceleration. The signals of these transducers were wired to a data acquisition system sampling at a frequency of 65,000 Hz. A high-speed camera (Fastcam SA1.1 by Photron®) was used to film the deformation-to-fracture process of the specimens. Images of the specimen deformation process from the high-speed camera were post-processed with an image tracking algorithm to derive the elongation of the specimens. The aperture of the lens selected for the high-speed camera was set to its widest opening, and the exposure time was balanced with the aperture. A 2000 W halogen light (LEIYING® M-300G) was installed to provide lighting for high-speed filming. The high-speed camera was set to film at 1000–8000 fps restricted by the camera capacity and lighting condition. The camera was synchronized using a TTL pulse generated by the INSTON testing machine.

The testing specimens were machined from 2.28 mm SGP sheet using a laser cutter and then polished along the edges. The geometry of the specimen needs to satisfy the following requirements: (1) the tensile region between the top and bottom clamps should be short enough to ensure the specimen fractures within the maximum stroke of the machine at highest testing speed; (2) the central testing gauge length should be sufficiently short to maximize the strain rate; (3) the radius of the shoulder should be large to avoid stress concentration; (4) the clamping region should be large enough to avoid specimen being pulled out from the taps; and (5) the area of the entire specimen should be minimized to reduce the weight so as to minimize the inertia effect. After examine all available testing standards [14–17] and recommendations [18], a few types of SGP specimens with different combinations of central gauge lengths, shoulder radii and tail lengths were made and then

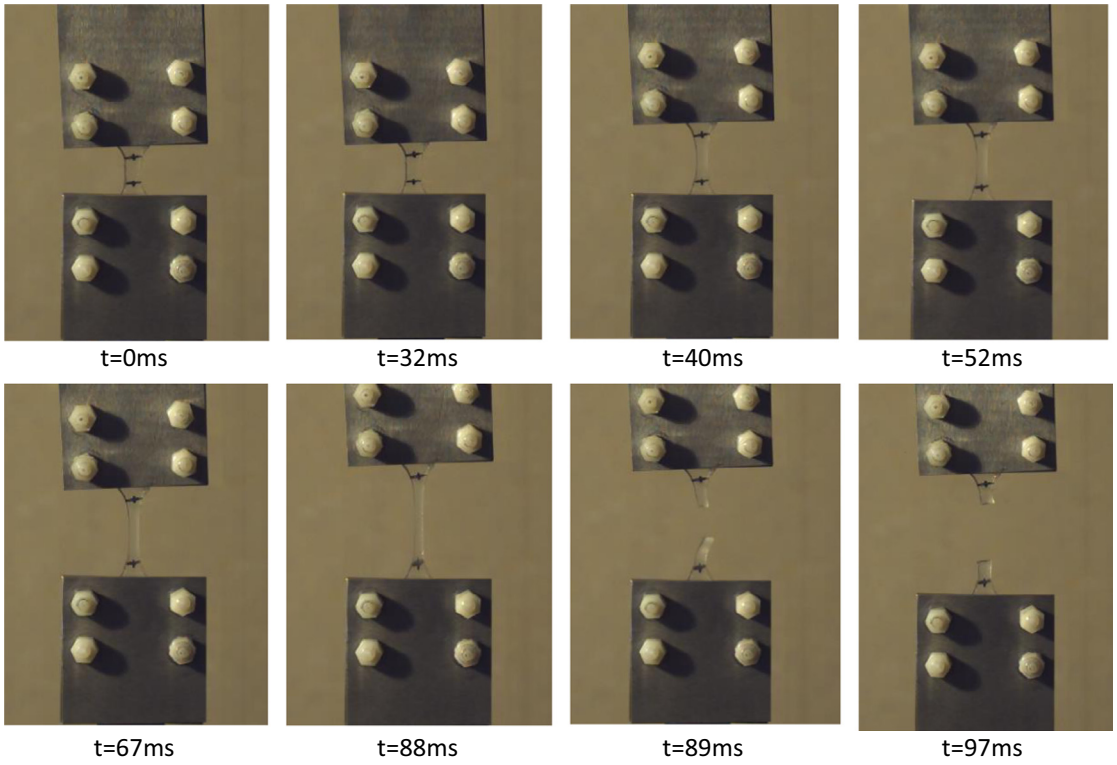


**Fig. 9.** High-speed camera images of specimen D05 deformation-to-failure process.

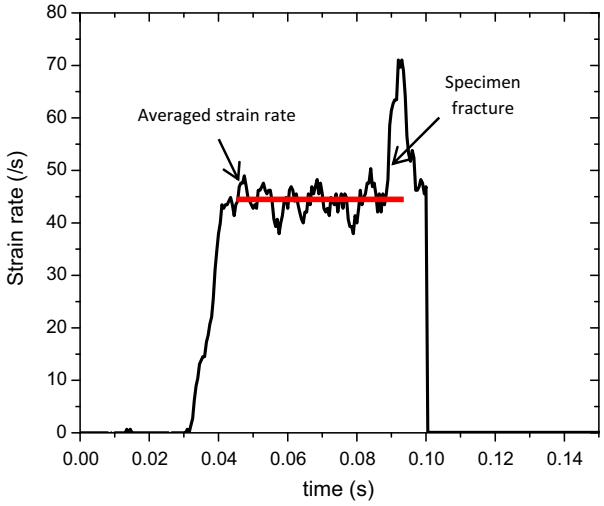


**Fig. 10.** Strain-rate time history of specimen D05 derived from high-speed imaging.

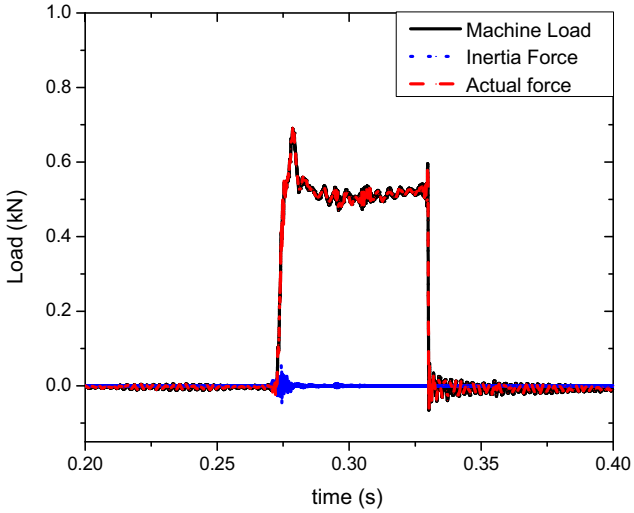


**Fig. 11.** Load time histories of machine load, inertia force, and actual force on material for specimen D05.

tried in preliminary testing. The geometry shown in Fig. 7 was identified to give the most satisfactory testing data. The specimen was cut into dumbbell shape with a central testing gauge of 10 mm in length. Two narrow black lines were drawn on each specimen as reference markers for the high-speed camera imaging. The engineering strain was calculated with the original testing gauge length between the reference markers, and the difference in length in the subsequent camera images. The radius of the specimen shoulder was modified after repeated tests, which showed that 9 mm was able to avoid stress concentration and consequential premature failure. 15 mm wide and approximately 45 mm long tails were provided at the both ends for clamping the specimen.

To reduce the inertia effect especially in the high-speed testing where the acceleration is large, lightweight clamps were specially designed and manufactured. The clamps were made of magnesium alloy (AZ31B). The density of magnesium alloy is 1.77 g/cm$^3$. The yield strength under direct tension is 200 MPa and the elastic modulus is 44.8 GPa, which ensure the clamping bars will not yield or experience large deformation when it is pulled in the high-speed tensile test. Lightweight plastic bolts (as shown in Fig. 8) made of PA-66 is utilized to fasten the alloy taps which firmly clamp the SGP specimen.

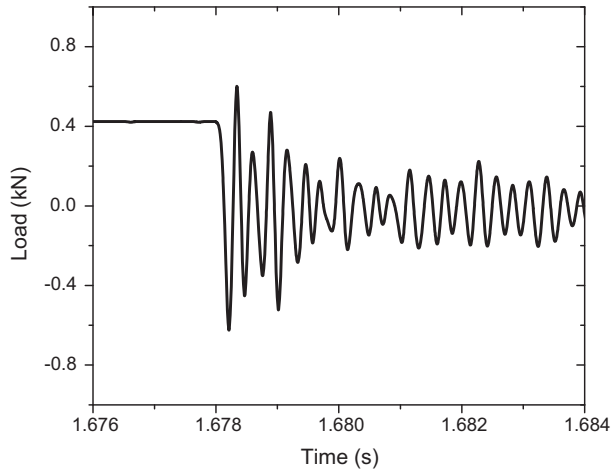


**Fig. 12.** Free vibration of the testing system after a specimen fractures.

### 4.2. Results

The testing results of the high-speed tensile tests are presented in the following section. Firstly, an example of high-speed test on SGP specimen D05 tested with an actuator speed of 0.5 m/s is presented to depict the deformation-to-failure process of the specimen and the strain rate time history that the specimen experienced with the aid of high-speed camera images. Demonstration is then given to show the contribution of inertia force and how the net force on the specimen is derived with the total load time history recorded by the load cell. Validation of dynamic stress equilibrium is performed. The testing data of all SGP specimens pulled at various speeds are then presented. The strain rate effect on SGP material is shown with engineering stress–strain curves at different strain rates.

#### 4.2.1. Deformation-to-failure process

Fig. 9 shows the high-speed camera images of the specimen deformation-to-failure process under the high-speed tensile loading. At $t = 0$ ms when the test initiated, the pistol was accelerated to the target testing velocity. The specimen was at rest as the moving jaw had not gripped the clamping bar. At $t = 32$ ms, the SGP specimen began to be stretched under the tensile force from the upper clamp. The specimen deformed quickly under tensile loading ($t = 40$–$87$ ms). At $t = 88$ ms, the specimen was greatly stretched with significant extension in length. Fracture initiated in the central region, which split the specimen into halves ($t = 89$ ms). The machine came to a rest after the specimen broke. It can be observed that after specimen breakage most of the extension of the stretched specimen recovered.

The vertical displacement trajectories of the specimen at the two black markers were traced by high-speed camera, which were post-processed and divided by the initial length of the testing gauge between the markers to derive the strain of specimen. Derivation was then made on strain time history to determine the strain rate that the specimen experienced. Fig. 10 shows the strain-rate time history for specimen D05. As can be seen, after the moving jaw grips the clamping bar which begins to pull the specimen upward, the strain rate of the specimen quickly increases to about 45 $s^{-1}$. A clear plateau can be found on the figure. At about 95 ms, the strain rate suddenly ascends again, indicating fracture of the specimen. The averaged strain rate on the plateau is slightly lower than nominal strain rate 50 $s^{-1}$ (0.5 m/s divided by 10 mm marked central testing gauge length). This is mainly because of the extension of the material at the shoulder of the specimen.

#### 4.2.2. Load time history and inertia effect

The load time history recorded by the load cell for specimen D05 is shown Fig. 11. To deduce the influence of inertia effect from the clamping devices, the inertia force is estimated by using the mass of clamp (including both the magnesium alloy bar and the plastic bolts) times the acceleration time history recorded by the accelerometer. A net force on the specimen is therefore obtained after subtracting the derived inertia force from the total force recorded by the load cell. As can be seen in Fig. 11, the contribution of inertia force is insignificant due to the light weight of the specially designed clamping device. Nonetheless, to obtain more accurate testing data, in this study the inertia forces in all the tests are removed from the recorded loads acting on the specimens.

#### 4.2.3. Validation of high speed test

To obtain valid testing data from high-speed dynamic test, the response of the entire testing system, i.e. the nature period of the load cell, the grips and the clamps, should be properly checked. Comparing with the rising time of the applied force onto the specimen, if the nature period of the system is not short enough, the measured force might not represent the true load applied to the specimen owing to interactions. Fig. 12 presents a load time history measured after a specimen breaks with the above test setup. From the figure it can be estimated that the nature oscillation period of the testing system is about 240 μs. When the actuator is pulling at a velocity of 0.5 m/s as shown above for specimen D05, the rise time of the tensile force to the point where specimen yielded is approximately 7200 μs, which is a lot longer than the nature period of the system. When the actuator pulling velocity increases to 10 m/s, the rise time is about three times the nature period of the system. When the actuator velocity reaches the maximum testing velocity of 20 m/s in this study, the rise time for the applied force to reach the yield stress of specimen is approximately 520 μs, which is the practical limit for the load cell being able to reliably track the material response [19]. Therefore in this study the testing velocity is limited to 20 m/s.

As mentioned in section two, in high-speed testing the condition of dynamic stress equilibrium should also be carefully checked to assure the measured data is valid. Moreover, during a high-speed test a sudden applied impulse can excite ringing of the testing system, which causes high amplitude stress oscillation and nonhomogeneous deformation in the specimen [12]. It is therefore important to ensure stress wave travel in round trips for a sufficient number of times in the specimen. The wave speed in the SGP material can be estimated using Eq. (2). If an averaged Young's modulus of 248 MPa resulted from the low-speed tensile tests in section three, and a material density of 0.95 $g/cm^3$ provided by DuPont® is used, the wave speed in the specimen is about 511 m/s. For a 20 mm testing length (between clamps) it takes about 39 μs for the stress wave to propagate through the specimen. For the above specimen D05, the fracture occurs at about 0.1 s as shown in Fig. 10, indicating the stress wave is able to propagate through the specimen for over 2500 times. Even at the maximum actuator pulling velocity, i.e., 20 m/s in this study, the stress wave could travel up and down within the specimen for more than six times. Therefore the condition of stress equilibrium is satisfied in the current tests, and the testing results measured are valid.

#### 4.2.4. Engineering stress vs. strain curves

Fig. 13 shows the engineering stress–strain curves for the SGP specimens tested at different actuator speeds, i.e. 0.1 m/s, 0.5 m/s, 1 m/s, 2 m/s, 3 m/s, 5 m/s, 7 m/s, 10 m/s, 15 m/s, and 20 m/s. As can be seen, under high deformation rates SGP still behaves as an elasto-plastic material. When actuator speeds are relatively low (0.1–3 m/s), SGP specimens respond very similarly to that under low-speed testing. There is a steep increase in stress

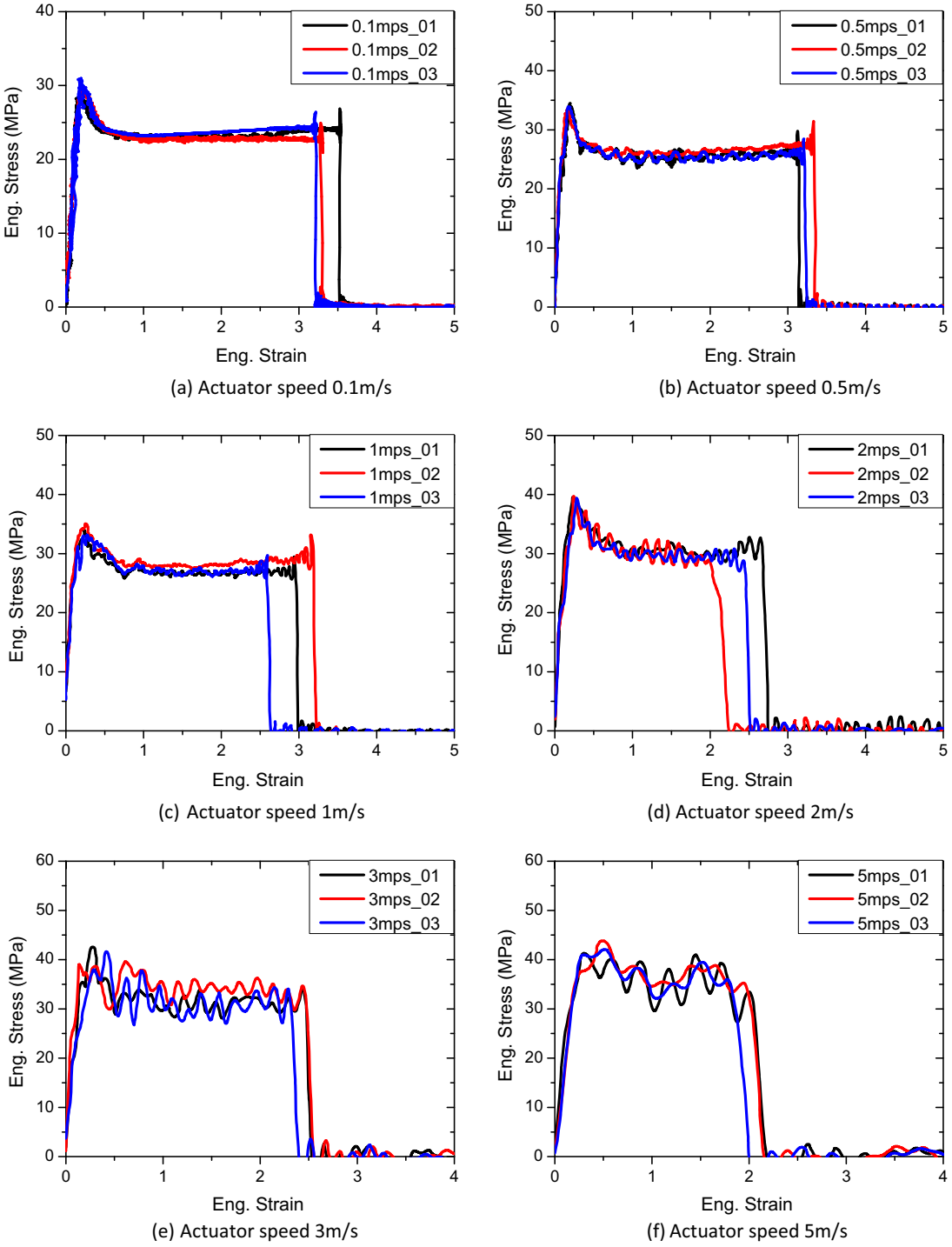


**Fig. 13.** Stress–strain curves of SGP in high-speed tensile tests.

at the beginning. After the stress reaches the peak value, it quickly plummets to a relative constant level, associated with a substantial plastic flow before ruptures. In comparison, when the actuator speeds are equal and higher than 5 m/s, SGP gradually show glassy behavior. After SGP yields, there is no more apparent drop in stress, and the plastic flow region becomes shorter as loading rate increases. Table 2 summarizes the testing results of SGP under high-speed uniaxial tensile loading. The yield stress, yield strain, initial modulus, failure stress, failure strain, as well as the actuator traveling speed, marker length, true strain rate derived from the high-speed camera images are listed. It can be found that the behavior of SGP is strain rate dependent in the high-strain rate range.

Fig. 14 shows the representative engineering stress–strain curves for SGP specimens tested at actuator speeds between 0.1 m/s and 20 m/s, which correspond to the strain rates between about 10 $s^{-1}$ and 2000 $s^{-1}$. Through comparison it can be found that the response of SGP material has strong strain rate dependence. At a strain rate around 10 $s^{-1}$ SGP material yields with a peak stress of about 29 MPa. As strain rates increases, the yield stresses increase. For instance, the yield stress increases to about 47 MPa when the strain rate is about 2000 $s^{-1}$. Moreover, as strain

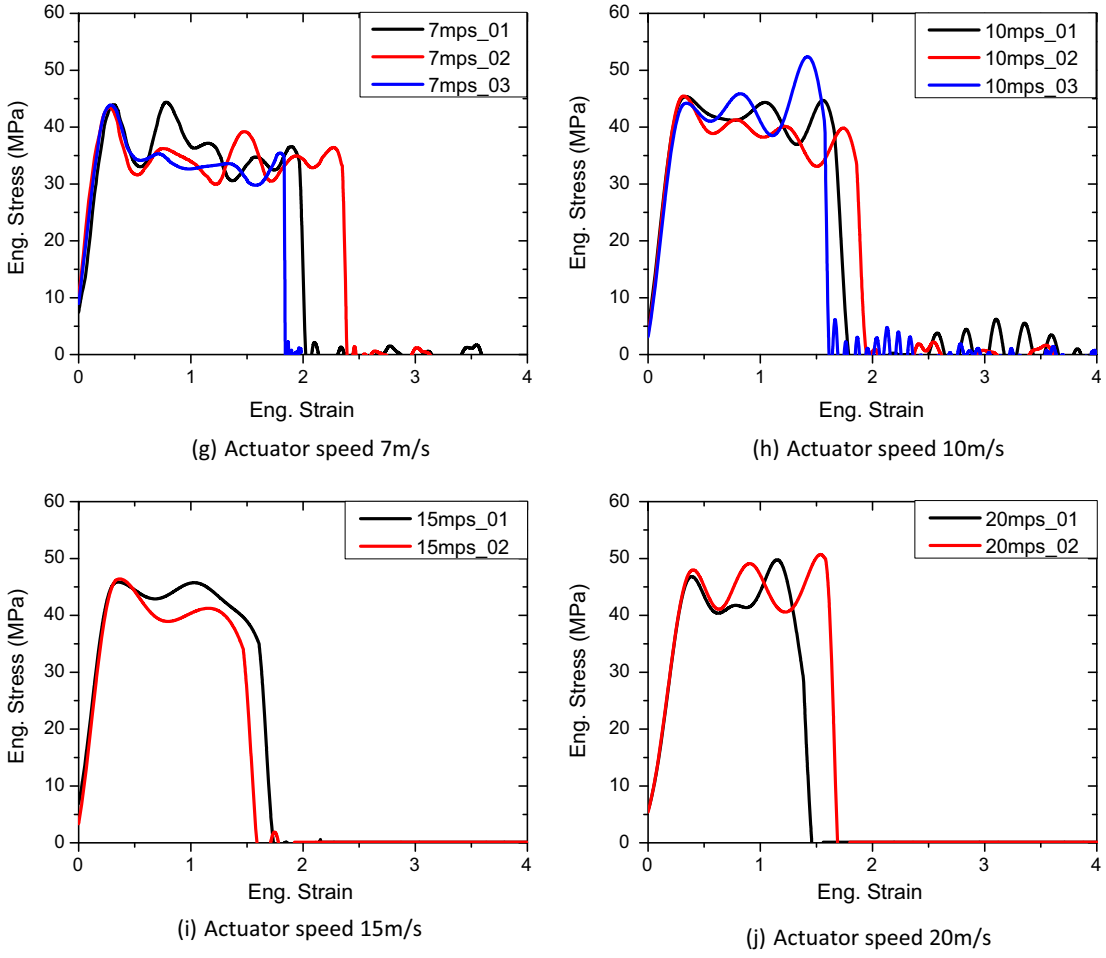


**Fig. 13** (*continued*)

**Table 2**
Summary of high speed tensile testing results.

| Test no. | Actuator speed (m/s) | Gauge length (mm) | Strain rate ($s^{-1}$) | Eng. $\sigma_{yield}$ (MPa) | Eng. $\varepsilon_{yield}$ | $E_{initial}$ (MPa) | Eng. $\sigma_{failure}$ (MPa) | Eng. $\varepsilon_{failure}$ |
|---|---|---|---|---|---|---|---|---|
| D01 | 0.1 | 9.02 | 10.58 | 28.33 | 0.17 | 168.00 | 24.30 | 3.65 |
| D02 | 0.1 | 10.63 | 10.36 | 29.20 | 0.18 | 158.34 | 22.85 | 3.39 |
| D03 | 0.1 | 9.87 | 10.96 | 30.97 | 0.18 | 171.51 | 24.66 | 3.22 |
| D05 | 0.5 | 10.94 | 48.97 | 34.51 | 0.20 | 176.07 | 27.08 | 3.11 |
| D06 | 0.5 | 10.94 | 45.17 | 33.61 | 0.19 | 180.73 | 38.22 | 3.32 |
| D07 | 0.5 | 10.00 | 49.26 | 33.91 | 0.18 | 193.76 | 26.84 | 3.20 |
| D08 | 1 | 10.00 | 100.00 | 33.96 | 0.24 | 141.52 | 28.03 | 2.95 |
| D09 | 1 | 8.68 | 109.13 | 35.06 | 0.25 | 139.11 | 30.73 | 3.19 |
| D10 | 1 | 8.96 | 105.83 | 33.17 | 0.27 | 122.39 | 28.22 | 2.59 |
| D13 | 2 | 10.70 | 240.00 | 39.58 | 0.23 | 169.14 | 32.38 | 2.65 |
| D14 | 2 | 10.25 | 231.85 | 39.71 | 0.23 | 173.39 | 29.43 | 2.00 |
| D15 | 2 | 10.67 | 222.78 | 39.35 | 0.28 | 140.93 | 30.75 | 2.46 |
| D16 | 3 | 11.01 | 321.38 | 42.57 | 0.26 | 161.61 | 32.99 | 2.42 |
| D17 | 3 | 10.77 | 316.43 | 39.64 | 0.27 | 147.76 | 34.36 | 2.45 |
| D18 | 3 | 10.32 | 330.25 | 41.64 | 0.28 | 149.00 | 33.95 | 2.29 |
| D19 | 5 | 10.18 | 531.43 | 41.30 | 0.28 | 147.51 | 33.43 | 2.01 |
| D20 | 5 | 8.98 | 597.50 | 43.83 | 0.29 | 153.75 | 35.25 | 1.96 |
| D21 | 5 | 9.05 | 607.50 | 42.08 | 0.28 | 148.47 | 35.95 | 2.00 |
| D24 | 7 | 10.45 | 716.30 | 44.36 | 0.30 | 149.09 | 36.49 | 1.94 |
| D25 | 7 | 9.94 | 736.15 | 43.48 | 0.27 | 159.24 | 36.35 | 2.26 |
| D26 | 7 | 11.08 | 684.48 | 43.88 | 0.30 | 148.00 | 35.29 | 1.78 |
| D27 | 10 | 8.62 | 1169.56 | 45.38 | 0.28 | 160.70 | 41.95 | 1.56 |
| D28 | 10 | 10.70 | 962.86 | 45.46 | 0.30 | 151.32 | 38.39 | 1.80 |
| D29 | 10 | 10.50 | 1005.36 | 44.20 | 0.32 | 138.96 | 40.68 | 1.57 |
| D30 | 15 | 10.99 | 1188.28 | 45.84 | 0.32 | 141.48 | 42.10 | 1.58 |
| D31 | 15 | 10.61 | 1453.67 | 46.39 | 0.33 | 142.75 | 40.15 | 1.51 |
| D33 | 20 | 10.08 | 2076.92 | 46.82 | 0.34 | 137.08 | 43.22 | 1.30 |
| D34 | 20 | 10.34 | 1873.87 | 47.99 | 0.36 | 135.15 | 45.54 | 1.47 |

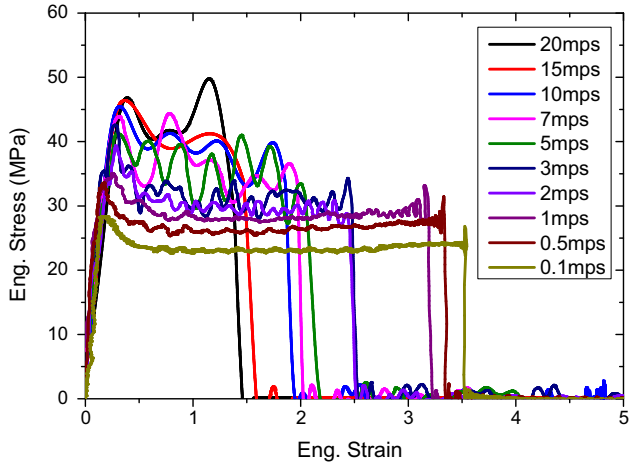


**Fig. 14.** Illustration of the strain rate effect on SGP material.

rate increases, SGP material becomes less ductile. At a strain rate of about 10 $s^{-1}$, SGP material breaks at an ultimate strain of about 350%. The failure strain reduces as strain rate increases. When the strain rate is 500 $s^{-1}$, the failure strain is only about 200%. It further drops to about 150% as material strain rate increases to about 2000 $s^{-1}$. It should be pointed out that the responses of SGP specimen at relatively high testing speeds (above 7 m/s) were associated with strong oscillations. This was because of relatively low strength of the SGP material and the vibration of the grip at high pulling speeds. The period of oscillations on load and displacement histories matched the natural period of the load cell and the grip. It should be noted that the raw data were filtered with a low pass filter with a cut-off frequency 2000 Hz when the actuator speed is higher than 7 m/s.

## 5. Analysis and discussion

### 5.1. Yield stress, yield strain and initial modulus vs. strain rates

The engineering stresses and strains at yield from both the low-speed and high-speed tests are presented in Figs. 15 and 16 as a function of strain rate. Previous testing data on SGP material by Bennison et al. [9] and Belis et al. [8] are also summarized and included for comparison and analysis. As can be seen, the yield stress shows a clear trend of increase with strain rate. At quasi-static state, the mean yield stress is approximately 22 MPa. The mean yield stress increases gradually with strain rate. When the strain rate is about 1 $s^{-1}$ the mean yield stress increases to about 30 MPa. When the strain rate rises to about 2000 $s^{-1}$, the mean yield stress increases to 47 MPa. The yield stresses from the current test agree well with the previous testing data. The increasing yield stress can be approximated by a bilinear trend line with the following equation

$$\sigma_y = 29.288 + 2.657\log_{10}\left(\frac{\dot{\varepsilon}}{\dot{\varepsilon}_0}\right) \quad \dot{\varepsilon} \leqslant 100\ s^{-1}$$
$$\sigma_y = 15.201 + 9.699\log_{10}\left(\frac{\dot{\varepsilon}}{\dot{\varepsilon}_0}\right) \quad \dot{\varepsilon} > 100\ s^{-1} \tag{4}$$

where $\sigma_y$ and $\dot{\varepsilon}$ are the yield stress and strain rate. $\dot{\varepsilon}_0$ is a reference strain rate of 1 $s^{-1}$.

The strain at yielding also increases with strain rate similar to that of yield stress. As shown in Fig. 16, the yielding strain is about 0.1 when the strain rate is about $10^{-2}$ $s^{-1}$. The yielding strain increases marginally as the strain rate increases to 1 $s^{-1}$. As the strain rate is greater than 10 $s^{-1}$, the yielding strain begins to rise quickly from about 0.17 to about 0.34 when the strain rate is about 2000 $s^{-1}$. The yield strains and yield stresses from the current tests agree with the previous testing data. A bilinear trend line similar to yield stress can be used to express yield strain

$$\varepsilon_y = 0.145 + 0.035\log_{10}\left(\frac{\dot{\varepsilon}}{\dot{\varepsilon}_0}\right) \quad \dot{\varepsilon} \leqslant 100\ s^{-1}$$
$$\varepsilon_y = 0.027 + 0.094\log_{10}\left(\frac{\dot{\varepsilon}}{\dot{\varepsilon}_0}\right) \quad \dot{\varepsilon} > 100\ s^{-1} \tag{5}$$

where $\varepsilon_y$ and $\dot{\varepsilon}$ are the yield strain and strain rate. $\dot{\varepsilon}_0$ is a reference strain rate of 1 $s^{-1}$.

Under uniaxial tensile loading, the stress of SGP material increases almost linearly with strain initially, and the stress–strain relationship becomes non-linear when the stress approaches the yield stress. In this study, however, the initial modulus, $E_{initial}$, is calculated as the secant modulus defined as the yield stress divided by the strain at yield. As shown in Fig. 17, when the strain rate is below 1 $s^{-1}$, the calculated initial modulus varies between 190 MPa and 320 MPa. The initial modulus in this strain rate range shows little strain rate dependency. As explained by Bennison et al. that SGP is a polymer material with a glass transition temperature of 55 °C. Below the glass transition temperature, the behavior of SGP including initial stiffness are insensitive to strain rate [9].

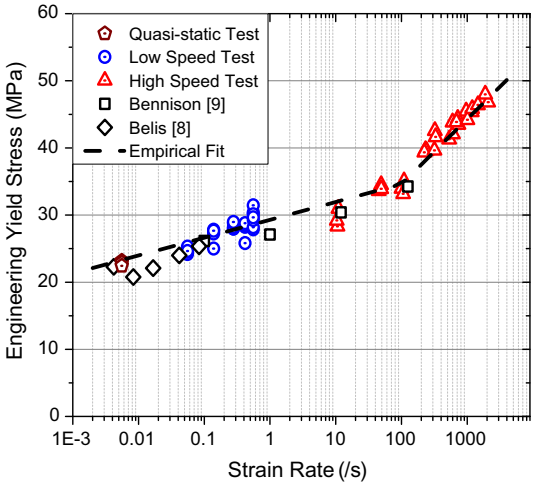


**Fig. 15.** Yield stress vs. strain rate.

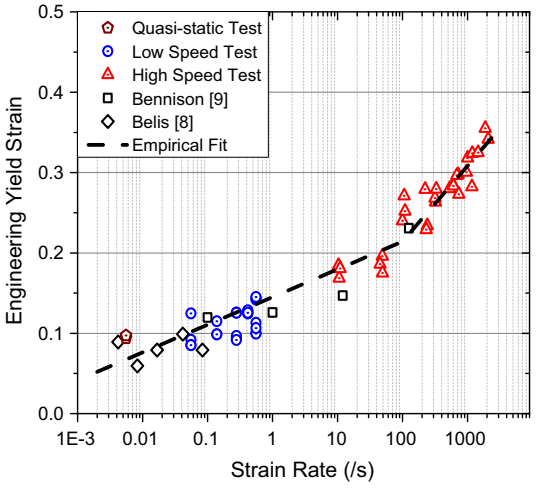


**Fig. 16.** Yield strain vs. strain rate.

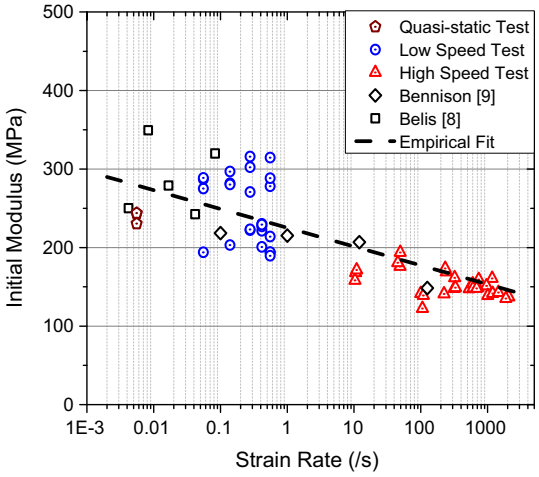


**Fig. 17.** Initial modulus vs. strain rate.

When strain rate is higher than 10 $s^{-1}$, the modulus is generally below 200 MPa and the values dwindle as strain rate increases. From the figure, it can be found that despite SGP material becomes more and more brittle as deformation rate increases, the initial modulus show a gradual decreasing trend as strain rate increases. The initial modulus $E_{initial}$ can be expressed as

$$E_{ini} = E_{ini,0} - m_E \log_{10}\left(\frac{\dot{\varepsilon}}{\dot{\varepsilon}_0}\right) \tag{6}$$

where $E_{ini}$ and $\dot{\varepsilon}$ are the initial modulus and the strain rate. $m_E$ is a constant, and $E_{ini,0}$ is the initial modulus at the reference strain rate $\dot{\varepsilon}_0$ of 1 $s^{-1}$. The constants were determined through nonlinear regression and were found to be $E_{ini,0}$ = 223.939 ± 4.389 MPa and $m_E$ = −27.449 ± 2.357 MPa.

### 5.2. Failure stress and strain vs. strain rates

Failure strains of SGP material at various strain rates are presented in Fig. 18. The failure strain of SGP material shows highly strain rate dependency. The quasi-static tensile tests carried out in the current study found the failure strains of the three specimens were all over 400%. As strain rate increases, the ductility of SGP material decreases. The failure strains of the SGP specimens involved in the low-speed tests fall in the range between 400% and 300% with a steady decreasing trend with strain rate. As strain rate increases to over 100 $s^{-1}$, SGP material becomes more and more brittle. The failure strain plummets as strain rate rises. At a strain rate of 100 $s^{-1}$, the mean failure strain is about 290%, and at 2000 $s^{-1}$ the mean failure strain reduces to below 150%. The failure strains can be fitted with a two-stage power equation as

$$\begin{aligned} \varepsilon_f &= 3.311 - 0.203\log_{10}\left(\frac{\dot{\varepsilon}}{\dot{\varepsilon}_0}\right) \quad \dot{\varepsilon} \leqslant 100\ s^{-1} \\ \varepsilon_f &= 4.9762 - 1.052\log_{10}\left(\frac{\dot{\varepsilon}}{\dot{\varepsilon}_0}\right) \quad \dot{\varepsilon} > 100\ s^{-1} \end{aligned} \tag{7}$$

where $\dot{\varepsilon}_0$ is a reference strain rate of 1 $s^{-1}$.

The true stress at failure instead of the engineering stress at failure is utilized for analysis. This is because the SGP specimens generally break at failure strains over 100% at high strain rates or even approaching 400% at low strain rates. Due to the significant elongations in length, the cross-sectional areas of specimens change greatly. Engineering stress at failure is therefore not an accurate measure to evaluate the stress differences between SGP specimens failed with different ultimate strains at various strain rates. The material true stress at failure is calculated using Eq. (3) and shown in Fig. 19. As shown, the true stresses at failure in the current test decrease slightly in the low strain rate range. The failure stress reduces from approximately 150 MPa at strain rate 0.0056 $s^{-1}$ to about 100 MPa when strain rate is 0.556 $s^{-1}$. The failure stresses remain almost a constant of about 110–120 MPa when strain rate is between 10 and 2000 $s^{-1}$. Similar observations were also obtained in the low strain-rate range by Belis et al. in their tests [8]. Variation can be observed between the current testing data and Bennison et al.'s results [9] when strain rate is above 1 $s^{-1}$. Since there is only one standalone testing data at each strain rate provided, and there is a lack of detail information about the testing setup such as specimen dimension, clamping method and etc. in reference [9], it is therefore difficult to evaluate the possible reasons for this variation. As previously mentioned by Xiao, because of the difficulties involved in high-speed tensile tests, such as system ringing, the influence of inertia effect, and etc., a round robin test involving 12 participating labs on five representative plastic materials found that the quality of testing data varied [12]. More high-speed tensile tests covering a wider strain rate range can be carried out to further verify the mechanical properties of SGP material. An expression similar to that for the failure strain can be utilized to describe the true stress at failure

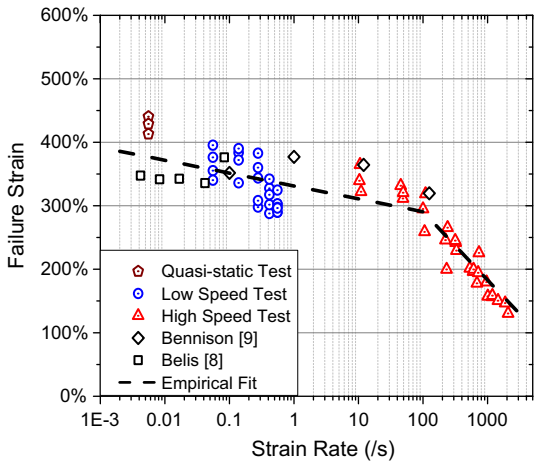


**Fig. 18.** Failure strain vs. strain rate.

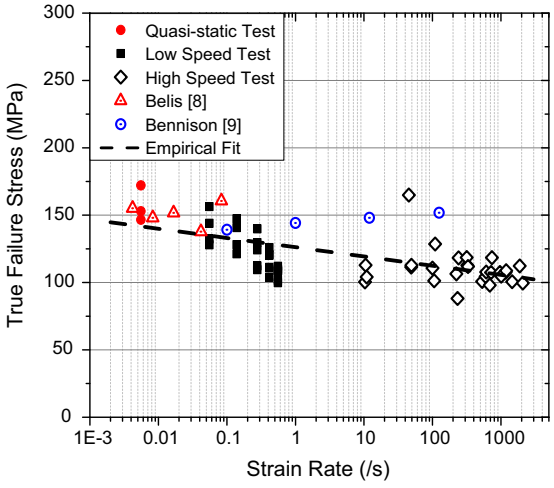


**Fig. 19.** True stress at failure vs. strain rate.

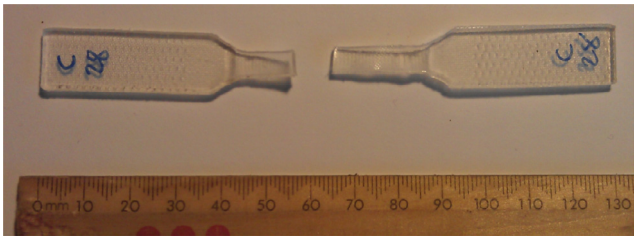

(a) Actuator speed 1000mm/min (SGP C28)

(b) Actuator speed 0.1~20m/sec

**Fig. 20.** Failure patterns of SGP specimens.

$$\sigma_{tf} = \sigma_{tf,0} - m_{tf}\log_{10}\left(\frac{\dot{\varepsilon}}{\dot{\varepsilon}_0}\right) \tag{8}$$

where $\sigma_{tf}$ and $\dot{\varepsilon}$ are the true failure stress and the strain rate. $m_{tf}$ is a constant, and $\sigma_{tf,0}$ is the failure stress at the reference strain rate $\dot{\varepsilon}_0$ of 1 $s^{-1}$. The constants were determined through nonlinear regression and were found to be $\sigma_{tf,0}$=126.207 ± 2.075 MPa and $m_{tf}$ = −6.857 MPa ± 1.115 MPa.

### 5.3. Failure pattern and plastic deformation

The stress–strain curves for SGP material indicate a typical elasto-plastic behavior in both the low-speed and high-speed tensile tests. Fig. 20 shows the failure patterns of the SGP specimens tested at various tensile speeds. At quasi-static state corresponding to a material strain rate about 0.0056 $s^{-1}$, substantial residual deformation was observed on the fractured specimen with a residual deformation of 263%. However, the maximum strain measured on the specimen B01 at failure is 413%. Even if the elastic strain of 9% at yielding is removed from the total achieved strain of 413%, the residual strain should still be 404%, substantially higher than 263%. This indicates approximately 35% of the maximum strain on the SGP specimen was recovered although it was associated with the plastic flow. This phenomenon is more apparent as strain rate increases. As shown in Fig. 20a, when the SGP specimen was pulled at 1000 mm/min (approx. $\dot{\varepsilon}$ = 0.556 $s^{-1}$), most of the extension was recovered. A permanent elongation of about 12 mm was measured on the fractured specimen, which indicates only 40% plastic strain although 296% maximum strain was measured when the specimen C28 was pulled to fracture. Similarly, as shown in Fig. 9 of the high-speed camera images, when pulled at 0.5 m/s actuator speed (approximate $\dot{\varepsilon}$ = 50 $s^{-1}$), the specimen experienced significant deformation. However, almost all this elongation was recovered after specimen breakage. Fig. 20b shows the fractured specimens involved in the high-speed testing at various speeds. Hardly any permanent extension can be found on any of these specimens, indicating the large deformation or flow is associated with the material viscous response, rather than plastic deformation when the loading rate is high.

## 6. Conclusion

This paper presents laboratory investigations on the dynamic material properties of ionoplast material SGP. Uniaxial tensile tests were performed covering a wide strain rate range from quasi-static state to a strain rate up to 2000 $s^{-1}$. The stress–strain curves show that SGP material exhibits an elasto-plastic behavior, which is also strain rate dependent. It was found that the yield stress varied from 22 MPa at a strain rate of 0.0056 $s^{-1}$ to 47 MPa at strain rate about 2000 $s^{-1}$. The corresponding yield strain was found to increase slightly over the tested strain rate range. The initial modulus of SGP was derived and found in the range of 200–300 MPa in low strain rate region and reducing to about 150 MPa in high strain rate range. The tests also found that SGP material became less ductile as strain rate increased. The failure strain reduced from about 400% at quasi-static state to about 150% at a strain rate of 2000 $s^{-1}$. The true stress at failure was found to vary between 90 MPa and 170 MPa. A slight decreasing trend was observed on the true stress in the low strain rate range, and the failure stress remains steady at a strain rate above 10 $s^{-1}$. Evaluation on the fractured specimens found the deformation was greatly recovered after specimens broke. The amounts of recovered deformation increase with the strain rate. The specimens tested under high-speed tensile loading retained literally no plastic deformations after specimen fractured. The observation indicated that SGP material showed viscous behavior under uniaxial tension.

## Acknowledgements

The authors would like to thank Australian Research Council for financial support. The contributions of final year student Mr. Todd Learmonth from the University of Western Australia and Mr. Xuejie Zhang from Tianjin University in conducting laboratory tests are acknowledged. We also acknowledge the supports from Cooling Brothers® Glass Company for providing testing materials. The first author would like to acknowledge the Ad Hoc scholarship from the University of Western Australia.

## References

[1] J.E. Minor, K.C. Mehta, Wind damage observations and implications, J. Struct. Div. 105 (1979) 2279–2291.

[2] X. Zhang, H. Hao, Z. Wang, Experimental investigation of monolithic tempered glass fragment characteristics subjected to blast loads, Eng. Struct. 75 (2014) 259–275.
[3] X. Zhang, H. Hao, G. Ma, Laboratory test and numerical simulation of laminated glass window vulnerability to debris impact, Int. J. Impact Eng 55 (2013) 49–62.
[4] X. Zhang, H. Hao, G. Ma, Parametric study of laminated glass window response to blast loads, Eng. Struct. 56 (2013) 1707–1717.
[5] X. Zhang, H. Hao, Laboratory test and numerical simulation of laminated glass window response to impact and blast loads, in: Proceedings of the 9th International Conference on Shock & Impact Loads on Structures, Fukuoka, Japan, 2011.
[6] P.A. Hooper, R.A.M. Sukhram, B.R.K. Blackman, J.P. Dear, On the blast resistance of laminated glass, Int. J. Solids Struct. 49 (2012) 899–918.
[7] M. Larcher, G. Solomos, F. Casadei, N. Gebbeken, Experimental and numerical investigations of laminated glass subjected to blast loading, Int. J. Impact Eng 39 (2012) 42–50.
[8] J. Belis, J. Depauw, D. Callewaert, D. Delincé, R. Van Impe, Failure mechanisms and residual capacity of annealed glass/SGP laminated beams at room temperature, Eng. Fail. Anal. 16 (2009) 1866–1875.
[9] S. Bennison, J. Sloan, D. Kistunas, P. Buehler, T. Amos, C. Smith, Laminated glass for blast mitigation: Role of interlayer properties, in: Proceedings of Glass Processing Days, Tampere, Finland, 2005.
[10] W.N. Sharpe Jr., W.N. Sharpe, Springer Handbook of Experimental Solid Mechanics, Springer, 2008.
[11] X. Zhang, Y. Zou, H. Hao, X. Li, G. Ma, K. Liu, Laboratory test on dynamic material properties of annealed float glass, Int. J. Protect. Struct. 3 (2012) 407–430.
[12] X. Xiao, Dynamic tensile testing of plastic materials, Polym. Testing 27 (2008) 164–178.
[13] J-2749, Hgih strain rate testing of polymers, SAE, 2006.
[14] BS ISO 37:2005, Rubber, vulcanized or thermoplastic. Determination of Tensile Stress–Strain Properties, London, 2005.
[15] ASTM D638-10, Standard Test Method for Tensile Properties of Plastics, West Conshohocken, PA, 2010.
[16] ISO 3537:1999, Road vehicles – Safety glazing materials – Mechanical tests, ISO, 1999.
[17] ISO 18872:2007, Plastics – Determination of tensile properties at high strain rates, ISO, 2007.
[18] M. Borsutzki, D. Cornette, Y. Kuriyama, A. Uenishi, B. Yan, E. Opbroek, Recommendations for dynamic tensile testing of sheet steels, Int. Iron Steel Inst. 30 (2005).
[19] P. Hooper, B. Blackman, J. Dear, The mechanical behaviour of poly (vinyl butyral) at different strain magnitudes and strain rates, J. Mater. Sci. 47 (2012) 3564–3576.